

15

Reducing Respiratory Artifacts in Thoracic PET/CT

Greta S.P. Mok, Tao Sun and Chi Liu

CONTENTS

15.1	Introduction	403
15.2	Breathing Instruction Based Methods.....	407
15.2.1	Shallow Breathing.....	407
15.2.2	Normal End-Expiration Breath-Hold.....	407
15.2.3	Deep-Inspiration Breath-Hold (DIBH) PET/CT.....	409
15.3	CT Protocol-Based Methods	410
15.3.1	Slow CT	410
15.3.2	Low-Pitch CT	411
15.3.3	Cine Average CT (CACT).....	411
15.3.4	Interpolated Average CT (IACT).....	413
15.4	Gated 4D PET/CT.....	414
15.4.1	Registration-Based Methods	415
15.4.2	Reconstruction-Based Methods.....	418
15.5	Deconvolution PET/CT	421
15.6	Conclusion	422
	Acknowledgments	423
	References.....	424

15.1 Introduction

It has been more than a decade since the introduction of the combined positron emission tomography and computed tomography (PET/CT) [1,2], which has been well recognized as the most sensitive tool for detecting neoplasm. The PET/CT technology, including detectors, reconstruction algorithms, and image analysis, matures over the years while researchers are still striving for better image quality and quantitation with lower radiation dose. To achieve this goal, various imaging degradation factors need to be compensated and we mainly focus on attenuation and respiratory motion blurring in this chapter.

For medical radionuclide imaging, the emitted gamma rays are attenuated in the body mainly via photoelectric absorption and Compton scattering before reaching the detectors. The photons originated from the center of the object would be more likely to be attenuated as compared to those that arise from the peripheral. Thus, this effect is positively related to patient body sizes and would contribute to gradually artifactual decrease of activity toward the center of the object. This effect is also more prominent for tracers with lower energy and for regions with higher attenuation coefficients, e.g., bone and metallic implants. Attenuation correction is critical for improving image quality and quantitation, and is the most important correction in PET.

Initial efforts of attenuation correction in emission tomography include conjugate-counting techniques especially using the geometric mean of the conjugate projections and the Chang's multiplicative method [3]. In the beginning, both methods assume a constant attenuation coefficient across the patient body, which is a reasonable estimate for brain and abdomen, to obtain the attenuation correction factor (ACF) by estimating the body thickness via the preliminary uncorrected images [4]. However, one may expect this assumption does not hold for most other regions like thorax and pelvis, where the presence of air and bone cannot be neglected. The urge of the attenuation coefficient for each voxel led to the requirement of an additional transmission scan.

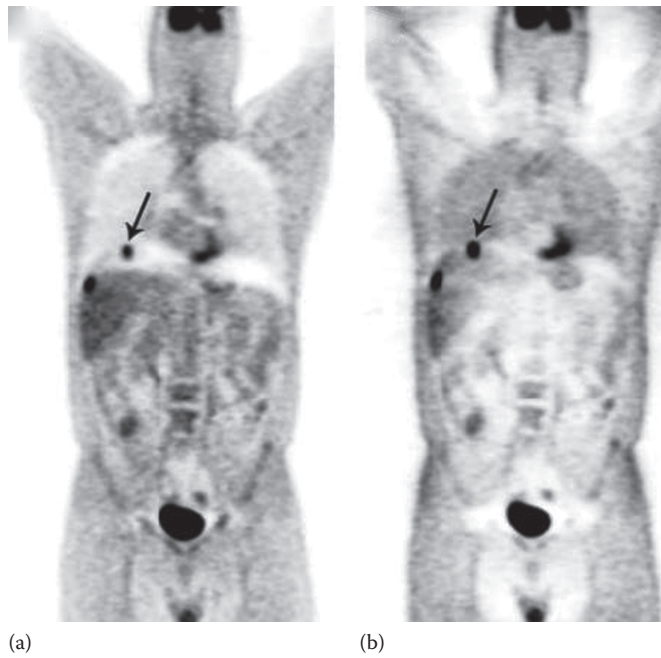
Before combined PET/CT scanners were invented, attenuation correction on standalone PET was performed mostly with an external ^{68}Ge 511-keV pin source that rotated around the patient. The pre-injection transmission scan required patients to stay on the bed of the scanner for the tracer distribution before the emission acquisition, thus limiting the patients' throughput. Though simultaneous acquisition with the emission scan was feasible [5], the post-injection transmission scan was usually performed right after the emission scan, thus saving a lot of time and also reducing the chances of patient movement between the transmission and the emission scans. However, the photons emitted from the patients could interfere with the transmission scan and degrade the count rate performance of the detectors. Thus, one needed to track the location of the external source and its targeted detectors for the transmission scan. The limited count rate of this transmission scan may substantially affect the quantitative accuracy or cause artifacts in the emission data [6]. The anatomical information provided by the transmission scan was also limited, thus it was not suitable for diagnostic purpose.

Nowadays, most clinical PET/CT machines no longer equipped with ^{68}Ge -based source. Instead, x-ray CT-based attenuation correction was commonly used in the combined PET/CT scanner [7]. This new design produced huge numbers of photons in the transmission scan even at low tube currents. Hence, it is much faster than the ^{68}Ge -based attenuation correction scan and has lower statistical noise level [8,9]. Also, CT-based attenuation correction ensures the significant energy difference between the gamma-rays (511 keV) and x-rays (~ 30 – 120 keV), so that the transmission scan would

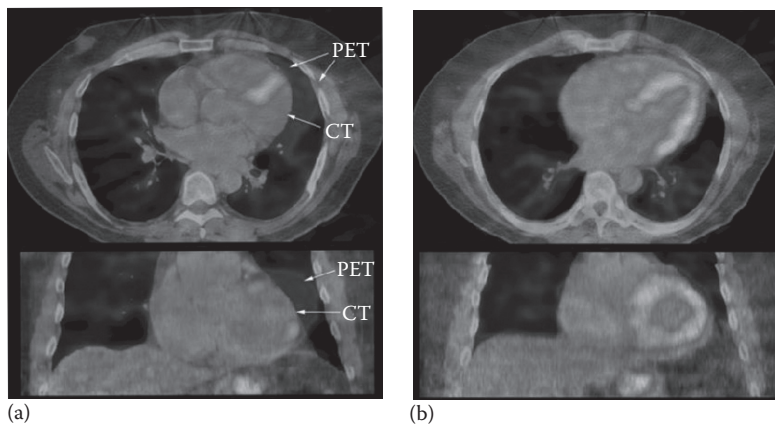
not be contaminated by the emitted gamma-rays from the patients. At the same time, it is necessary to transform the CT images acquired from an integrated energy spectrum of $\sim 30\text{--}120$ keV to attenuation maps of 511 keV for attenuation correction in the emission data. This conversion usually involves segmentation of bone and nonbone materials, and/or applying the bilinear scaling methods [8,10]. The use of CT-based attenuation maps leads to a more accurate activity concentration values and better uniformity [11], and provides more anatomical information for the correspondingly registered emission data.

On the other hand, CT-based attenuation correction for PET is hampered by artifacts that are usually not seen in the standalone PET images. Examples are artifacts due to respiratory motion [12–14], truncation [15], metallic implants [16,17], and CT contrast agents [18,19]. Among all these factors, respiratory motion is generally considered to be the main problem in CT-based attenuation correction. For standalone diagnostic CT, the optimized protocol is to obtain a 3D helical acquisition of the thoracic cavity over a single full-inspiration breath-hold CT scan. When applied with the emission exam, this technique captures a snapshot of the thoracic cavity at a distinct respiratory phase and does not represent the time-averaged position of the thoracic structures as PET acquisition does. This misalignment between transmission and emission scan is most noticeable at the left lung especially for two regions: (i) tissues around lower thorax and upper abdomen, where the transmission scan may not be presented in the emission scan (Figure 15.1); (ii) tissues around the lung and left-ventricle interface, where myocardial uptake is prominent overlying the left lung of the CT in the fused images (Figure 15.2). In fact, for thoracic structures, more than 40% of the studies have misalignments between the measured and the true position [20]. Erdi et al. examined PET/CT images of five patients with multiple lung carcinoma lesions, and showed that the spatial mismatch resulted in up to a 30% error in the standardized uptake value (SUV) of the lesions [21]. Also, phantom studies showed the effect of motion can result in as much as 75% underestimation of the maximum activity concentrations [22]. In a simulation study with over 1000 real patient respiratory traces, in addition to SUV underestimation caused by motion blurring, mismatched attenuation correction can cause SUV overestimation for lower lung tumors which are close to the liver dome, leading to complicated SUV errors [23]. These PET/CT mismatch artifacts may lead to inaccurate localization of tumors and hence potential misdiagnoses [13,24,25].

Besides the matching of PET and CT data, the respiratory motion during PET acquisition itself also causes substantial degradations of spatial resolution, contrast-to-noise ratio, size and shape of the lesions, and quantitative accuracy. For PET/CT-guided radiotherapy, it can cause the tumor size to be overestimated by up to 130% [23], thus increasing the planning target volume. Dawood et al. showed that the respiratory motion can cause the thoracic/abdominal tumors to move with an amplitude of $\sim 6\text{--}23$ mm [26],

**FIGURE 15.1**

PET reconstructed images of a 58-year-old man with colon cancer. (a) A lesion at the dome of liver was mislocalized to right lung (arrow) because of the respiratory motion. (b) Images without attenuation correction showed that all lesions were confined to the liver. (Reprinted from Sureshbabu, W. and Mawlawi, O., *J. Nucl. Med. Technol.*, 2005, 33(3), 156. With permission.)

**FIGURE 15.2**

(See color insert.) (a) Helical CT and PET fusion images in transaxial (top) and coronal (bottom) views showed marked misregistration. Arrows indicated the mismatch of heart borders between the helical CT and the PET images, and an artifactual defect in the myocardium. (b) For the same patient, cine average CT and PET fusion images showed no misregistration and artifactual defects. (Reprinted from Gould, K.L. et al., *J. Nucl. Med.*, 2007, 48(7), 1112. With permission.)

and Erdi et al. demonstrated that the degree of blurring is proportional to the breathing magnitude [27]. Xu et al. showed that the blur extent was about 12.1 ± 3.7 mm in their blur reduction study [28].

Effective methods are warranted to reduce the PET/CT respiratory artifacts. Three main categories of these methods have been mostly investigated so far: breathing instruction, CT protocols, and gated four-dimensional (4D) PET/CT.



15.2 Breathing Instruction Based Methods

15.2.1 Shallow Breathing

Instead of deep-inspiration breath-hold protocol in diagnostic CT, some studies acquire both CT and PET under continuous shallow breathing state, which has relatively smaller motion amplitudes. However, studies showed that this protocol resulted in an unsatisfactory evaluation of the lung parenchyma on CT images (Figure 15.3), where subcentimeter nodules can be missed to cause inaccurate comprehensive cancer staging [29].

Multidetector CT technology that employs six or more detector rows can reduce magnitude and frequency of respiratory artifacts in free breathing PET/CT [30]. This is because, with multidetector CT technology, the CT examination time of whole-body PET/CT scan is shortened to 20 s or less. Thus, patients' irregular breathing pattern will be significantly mitigated.

15.2.2 Normal End-Expiration Breath-Hold

Some researchers believe normal end-expiration breath-hold is the best option for transmission scan in thoracic PET/CT [31,32]. In a survey performed

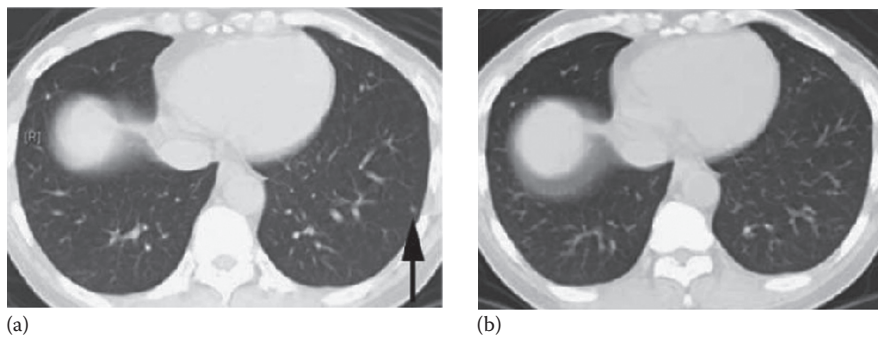


FIGURE 15.3

A 4-mm nodule in left lower lobe of lung (arrow) was seen on (a) deep-inspiration breath-hold CT, but was missed on (b) shallow-breathing CT for a patient with pancreatic cancer. (Reprinted from Allen-Auerbach, M. et al., *J. Nucl. Med.*, 2006, 47(2), 298. With permission.)

by Goerres et al. [10], CT scans were performed at four respiratory levels: free-breathing, maximal-inspiration, maximal-expiration, and normal-expiration. For different breathing protocols, multiple distances between the anatomical landmarks or a reference point in the CT and corresponding PET images were compared. Normal-expiration breath-hold showed the best results with better match and smaller range of measured distances as compared to other breathing patterns for the upper abdominal organs. Furthermore, this CT protocol reduced the occurrence and the severity of respiratory curvilinear artifacts on co-registered PET/CT images. Another study showed that reconstructed images from patients of normal-expiration breath-hold group had 28% less incidence rate of artifacts as compared with those from the free-breathing group [32]. One possible explanation is that a normal human spends most time in expiration in the whole respiratory cycle. Further comparison study showed that normal-expiration CT scan for attenuation correction gave good SUV recovery in the case of mobile tumors with size of 20 mm, even when the magnitude of breathing was large [33]. Attenuation correction using maximal-inspiration breath-hold protocol resulted in more serious underestimation of SUV, especially when breathing amplitude increased.

The clinical challenge of normal end-expiration breath-hold protocol is patient's compliance and comfort. The procedure needs to be rehearsed before transmission scan. Many patients are incapable of maintaining breath-hold for the duration of the whole-body CT examination, even for the most advanced multidetector CT scanner. It has been reported that 40%–60% patients with lung cancer are unable to consistently hold their breath for a long period [34]. This results in severe compensatory breathing artifacts at the midscan level, i.e., the lower thorax to the upper abdomen region, when the patient resumes breathing during the CT acquisition. These patients are suggested to use the shallow breathing protocol instead.

Even under the assumption of successful breath-hold, it is still doubtful if the normal end-expiration breath-hold CT will match with the PET data as it is difficult to instruct the patient to obtain a predefined position of the diaphragm. Furthermore, the shape of the diaphragm in normal end-expiration may differ from the free breathing in the PET acquisition, as breath-holding may generate different muscle tension [35] as in the free breathing state. Active expiration breath-hold originates from the muscles of the chest wall, and thus will push up the diaphragm and generate an abnormal shape of the diaphragm as compared to normal expiration without breath-holding. Also, normal end-expiration breath-hold CT still captures a snapshot of the thoracic cavity in a distinct respiratory phase and does not represent the time-averaged position of the thoracic structures as PET acquisition does. Hamill et al. [33] indicated good SUV recovery of normal-end expiration was actually due to canceling effects of underestimation due to motion blurring and overestimation due to attenuation. For small lung tumors near the diaphragm, their phantom study showed the inaccurate estimation of SUV after attenuation correction with normal-end expiration CT.

15.2.3 Deep-Inspiration Breath-Hold (DIBH) PET/CT

Nehmeh et al. proposed a deep-inspiration breath-hold protocol for both CT and PET (DIBH PET/CT) acquisition [36]. The patient was instructed to breathe deeply and then hold the breath, under the monitoring with an amplitude gating device, i.e., the real-time position management (RPM, Varian Medical Systems, Palo Alto, CA). Breath-hold CT data were acquired for about 16 s in the helical mode. PET scan was divided to nine 20 s frames, i.e., with a total acquisition of 3 min for one bed position. In the beginning of each PET frame, patient was instructed to breathe and hold the breath again as in DIBH CT. The inflation level was defined on the fly during DIBH CT session. The breath-hold signal exhibited a relaxation period of 1–2 s before it stabilized. Therefore, it was necessary to wait for 1–2 s before starting the acquisition. PET data were acquired for only one bed position. The whole process was shown in Figure 15.4. This method showed an increase in lesion

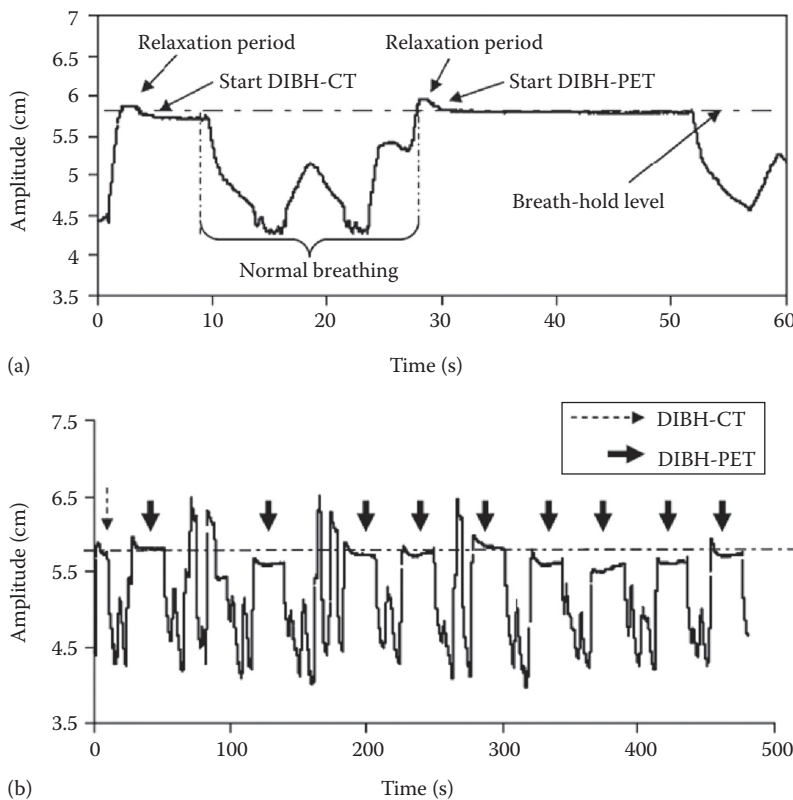


FIGURE 15.4

RPM breathing signals of a patient undergoing DIBH PET/CT acquisition mode. (a) The patient first did the breath-hold on CT and then started the first PET frame. Dashed line corresponded to the inflation level at which patient was instructed to hold the breath. (b) The whole DIBH PET/CT session. (Reprinted from Nehmeh, S.A. et al., *J. Nucl. Med.*, 2007, 48(1), 22. With permission.)

SUV of as much as 83% and a reduction in the distance between the centroids of PET and CT lesions as much as 49%, compared to the deep-inspiration breath-hold PET/CT. Similar study was proposed by Meirelles et al. [37] and Torizuka et al. [38]. They both showed increase in SUV and more precise localization and quantification of lesions when using the DIBH PET/CT technique. Better diagnostic accuracy can be achieved by using DIBH PET with a single 30 s, 45 s, or even 60 s scan in one frame [39,40].

By now, the DIBH PET/CT method was only explored in lung lesion studies. Additional external monitoring such as RPM and breathe-coaching are also needed to measure the respiratory cycle, ensuring the matching of the transmission and the emission respiratory phases. However, even a single breath-hold for 20 s may not be acceptable for senior patients or patients who have underlying lung diseases such as emphysema or pulmonary fibrosis [38]. Unsuccessful breath-hold due to irregular breathing pattern may cause highly variable results, which will affect the diagnostic accuracy.

15.3 CT Protocol-Based Methods

There are two main scan modes for CT acquisition, the axial (step-and-shoot) mode and the helical (spiral) mode. The step-and-shoot CT consists of two stages: (i) the patient remains stationary while the x-ray tube and gantry rotate around the patient to acquire a complete set of projections at a prescribed scanning location; (ii) the tube is off and the patient is translated to the next prescribed axial scanning location. The duty cycle (scan time/total time) of the step-and-shoot CT is ~50% at best. The helical CT [41,42] was then introduced to solve the interscan missing problem as in the step-and-shoot CT. The CT data are acquired while the patient is continuously transported through the gantry with a constant speed. The duty cycle of the helical CT is nearly 100%. As the scanning speed performance can be substantially improved, the scanner is able to image a given volume in a shorter time as compared to the step-and-shoot mode.

Specific CT protocols based on the axial mode or helical mode have been proposed for attenuation correction in PET images, with the same idea to acquire CT data over many respiratory cycles to ensure the CT attenuation map matches with the PET. Thus, breathing-induced artifacts such as PET/CT spatial mismatch and underestimation of the SUV would be reduced.

15.3.1 Slow CT

Lagerwaard et al. introduced slow CT under helical mode to average several respiratory cycles over the scan duration [43]. The tube rotation time of a single-slice CT was slowed down to 4 s/rot. Pitch was set to 1. Compared

with the diagnostic deep-inspiration breath-hold CT, slow CT was closer to the average position of the thoracic cavity structures in PET.

In another study from Sorensen et al. [44], severe “gap” artifacts between successive PET reconstructed slices using slow CT-based attenuation correction were observed. It was possibly due to the inconsistencies in the projections from large respiratory motions combined with slow CT propagated into the attenuation-corrected PET images. Hence, this method may not be appropriate for attenuation correction in PET/CT for large respiratory motion amplitudes.

15.3.2 Low-Pitch CT

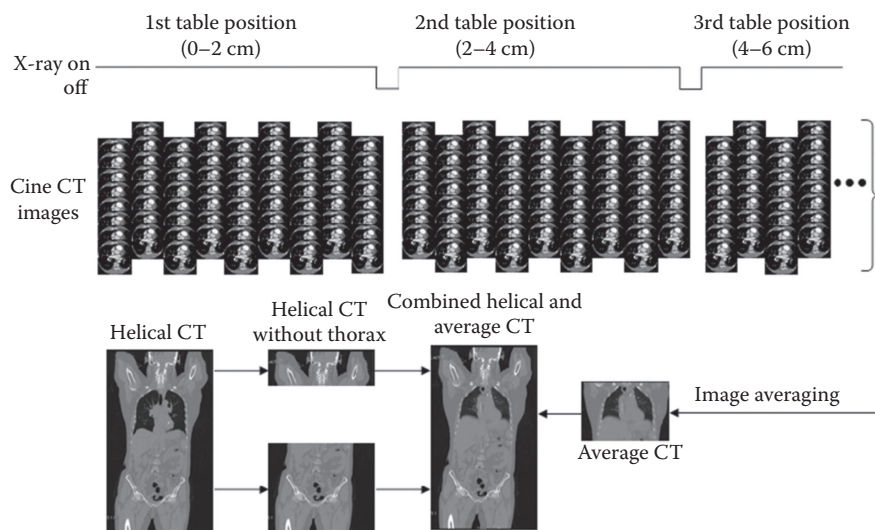
New generations of CT provide more configurations for helical mode. Nye et al. set the pitch as 0.562, which was the lowest value allowed by the scanner [45]. This pitch value increased the axial sampling during free-breathing mode without increasing the tube rotation time. A total of 16 s scan was used to cover the chest cavity. Final CT data were matched with the PET slice thickness for attenuation correction and to suppress respiratory motion artifacts. Compared to deep-inspiration breath-hold CT, this low-pitch CT reduced the number of problematic studies from 71% to 28%.

One concern for low-pitch CT is the radiation burden. Due to the potential longer exposure time, higher radiation dose is delivered to the patients for the low-pitch CT. The radiation dose was approximately 2.3 mSv as compared to a 1.8 mSv of the diagnostic breath-hold CT. The dose length product was 153 mGy, also higher than the conventional method of 117 mGy [45]. The relative high radiation dose hampers the low-pitch CT from common clinical applications.

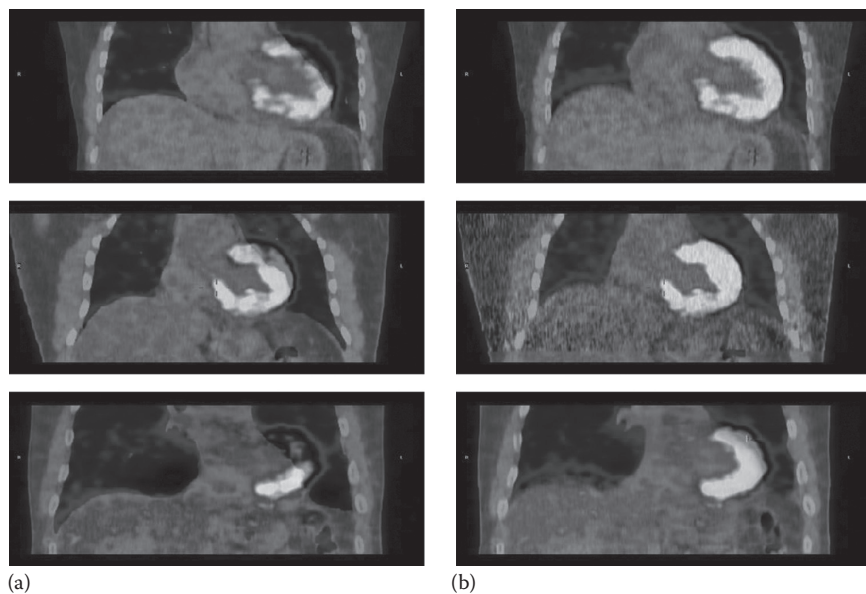
15.3.3 Cine Average CT (CACT)

Pan et al. introduced 4D CT for PET/CT attenuation correction [46], see Chapter 7 in this book. 4D CT provided images of all phases of the breathing cycle for tumor staging and radiation therapy treatment planning [47]. Cine mode technique, modified from step-and-shoot mode, acquired repeated axial CT images at each table position for a certain time period. This method produced even thinner slice thickness than those of a low-pitch helical scan.

Pan et al. [46,48] and Cook et al. [49] averaged the images of 10 phases in 4D CT to form a respiratory cine average CT (CACT) at each table position (Figure 15.5) to cover the whole thorax region. The acquisition time for each table position is 5.9 s. The average CT of the thorax was then combined with the helical CT data of the regions outside the thorax, e.g., abdomen, to make up the integrative CT images. This method greatly improved the registration accuracy and tumor SUV as compared to attenuation correction using deep-inspiration or normal end-expiration breath-hold helical CTs (Figure 15.6). Similar results were achieved by Gould et al. [20].

**FIGURE 15.5**

Top row: After cine scan at the first location, the table travels another 2 cm. After averaging the cine images, a full set of CT images can then be formed by combining the helical CT images above and below the thorax and the CACT images of the thorax for attenuation correction in the PET emission data. (Reprinted from Pan, T. et al., *Med. Phys.*, 2006, 33(10), 3931. With permission.)

**FIGURE 15.6**

(See color insert.) Fused coronal images of the PET data with (a) helical CT and (b) CACT for two different patients. (Reprinted from Pan, T. et al., *Med. Phys.*, 2006, 33(10), 3931. With permission.)

Alessio et al. further evaluated both average and intensity maximum images of 4D CT for the PET/CT misalignment reductions [50]. Fewer misalignments were observed with intensity-maximum 4D CT. Moreover, compared to helical CT, 4D CT was more flexible to be retrospectively averaged or processed.

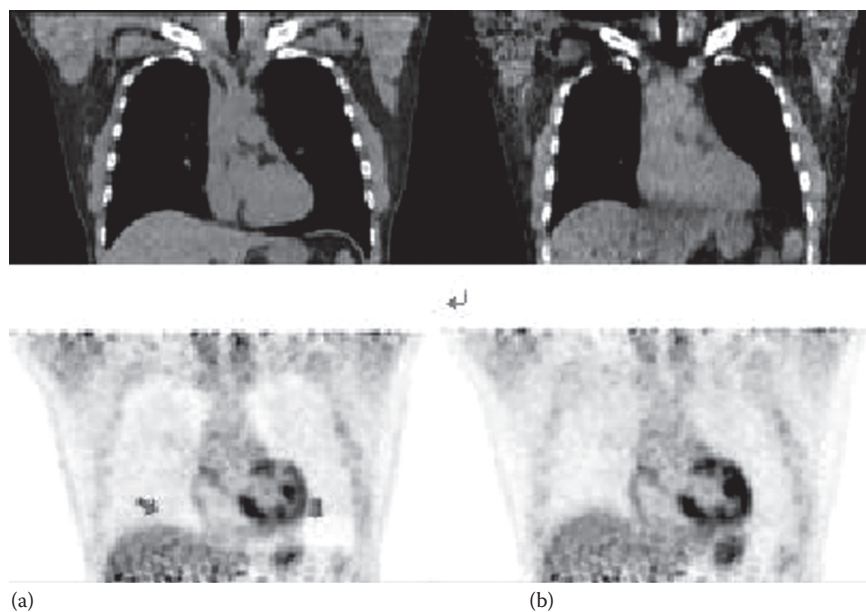
There are mainly two adverse problems for CACT: (i) increasing the CT acquisition time due to the longer period of each bed position; (ii) increasing the radiation dose. Lowering the tube current can potentially reduce the dose by a wide margin [48].

15.3.4 Interpolated Average CT (IACT)

An alternative method for CACT is interpolated average CT (IACT) to reduce radiation dose with similar image quality [51]. CT images of desired phases, e.g., end-inspiration and end-expiration phases from a respiratory cycle, are used to generate the velocity matrix using deformable image registrations such as optical flow method (OFM) [52] or B-splines. Interpolated phases are then obtained via linear interpolations or based on the organ movement functions [53]. The IACT is then calculated by averaging the original and interpolated phases. In a clinical study, Huang et al. obtained the IACTs using different numbers of desired phases from a cine CT [51]. The PET images were then reconstructed using different IACTs, CACT, and helical CT for attenuation correction. The maximum SUV difference between the use of IACT and CACT was about 3%. The radiation dose using IACT with two original phases, i.e., end-expiration and end-inspiration, could be potentially reduced by 85% as compared to the use of CACT.

A further simulation study showed that IACT was a robust method that worked for maximum respiratory motion amplitude of up to ~ 3 cm [54]. Another study investigated the clinical feasibility of IACT and its potential radiation dose reduction using an active breathing controller (ABC) [55]. If the CT scans were acquired during the voluntary breath-holds performed by the patients themselves, they could probably not represent the normal breathing state as in the PET acquisition. Thus, the ABC was introduced to capture the desired breathing phases. It is a noninvasive device that integrated a spirometer, an air mask, and a tube-valve system. The user can manually close the valve depending on the read-in breathing signal to suspend the patient's breathing for a desired period of time (<10 s). The results in a preliminary clinical study showed that IACT using ABC provided improved image quality as compared to conventional helical CT (Figure 15.7).

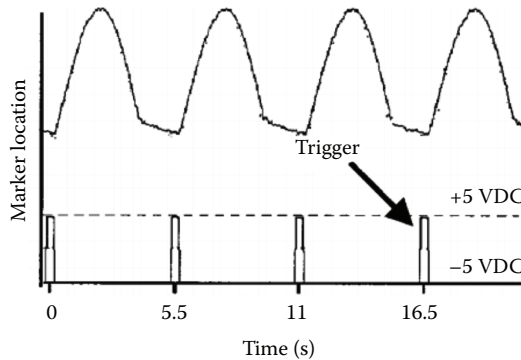
The aforementioned methods all aimed to correct the misalignments between PET and CT by modifying the CT images to match with the PET images. However, respiratory motion blur always exists in the static PET, and it cannot be compensated by only matching the CT with the static PET images. The following techniques aim to correct the motion blurring by further processing the PET raw data or reconstructed images.

**FIGURE 15.7**

(a) Sample images of helical CT (top) and its corresponding PET reconstructed images (bottom). (b) Sample images of IACT (top) and its corresponding PET reconstructed images (bottom). Red arrows: misalignment artifacts (From Sun, T. et al. Low dose interpolated average CT for PET/CT attenuation correction using an Active Breathing Controller (ABC), paper accepted for presentation in *IEEE Nuclear Science Symposium Medical Imaging Conference*, Anaheim, CA, October 28–November 3, 2012.).

15.4 Gated 4D PET/CT

Respiratory gated PET was firstly proposed for the standalone PET in brain scan to remove patient motions [56]. To reduce smearing due to the breathing motions and improve quantification of ^{18}F -FDG uptake in lung lesions, Nehmeh et al. proposed respiratory gated PET [57]. PET data were acquired into discrete bins in synchrony with the breathing cycle. In this study, 10 bins data were acquired for a FOV, with 300–500 ms time interval between each 1 min gated bin (Figure 15.8). The lesion motion was negligible due to the short acquisition interval and thereby approximately motion-free images were obtained. During the gated PET acquisition, different respiratory tracking systems, such as RPM, pressure-monitor belt, and spirometer, have been used to monitor the respiratory motion and generate a trigger for the PET scan at predefined amplitude or time phase. Studies using this technique showed an improvement in the target-to-background ratio and a more accurate measurement of the SUV [57,58].

**FIGURE 15.8**

Respiratory gating signals indicated by RPM marker location and the corresponding electrical triggers for PET acquisition. (Reprinted from Nehmeh, S.A. et al., *Med. Phys.*, 2002, 29(3), 366. With permission.)

Each gated PET image is usually directly corrected by an unsynchronized breath-hold CT. Hence, the reconstructed image quality in some gates is even worse than those of the non-gated PET with attenuation correction by a conventional breath-hold CT due to worse mismatch. Instead of manipulating CT protocols to match the static PET, 4D PET/CT applied 4D CT on gated PET images to facilitate phase-matched CT-based attenuation correction.

In 4D PET/CT imaging, the previously described 4D CT and gated PET are combined [59]: the 4D CT images are spatially matched with the gated PET images. In synchrony with the externally monitored breathing signal, respiratory gated PET data are acquired into discrete bins. 4D CT data are acquired and sorted according to their phases to generate a respiratory gated CT data. To make the CT images in each phase coincide with the PET images, the gated CT images at each bin are then spatially rebinned and resliced in the axial direction. The gated PET data are then corrected for attenuation with the corresponding gated CT data.

In a clinical study, Nehmeh et al. measured distances of the lesion centroids between the gated PET and the phase matched 4D CT [59]. The result showed an improvement in lesion registration of PET and CT up to 41% as compared to the registration between gated PET and deep-inspiration breath-hold CT (Figure 15.9). Also, a reduction in PET derived tumor volumes of up to 42% and an increase in lesion SUV of up to 16% were also found. Similar studies [60–63] all showed that 4D PET/CT provided superior results as compared to gated/non-gated PET with a breath-hold CT for attenuation correction.

15.4.1 Registration-Based Methods

One may notice that in 4D PET/CT, each PET bin only contains a small fraction of detected PET events. The resultant reconstructed images, therefore, have higher noise level, thus a poor signal-to-noise ratio (SNR).

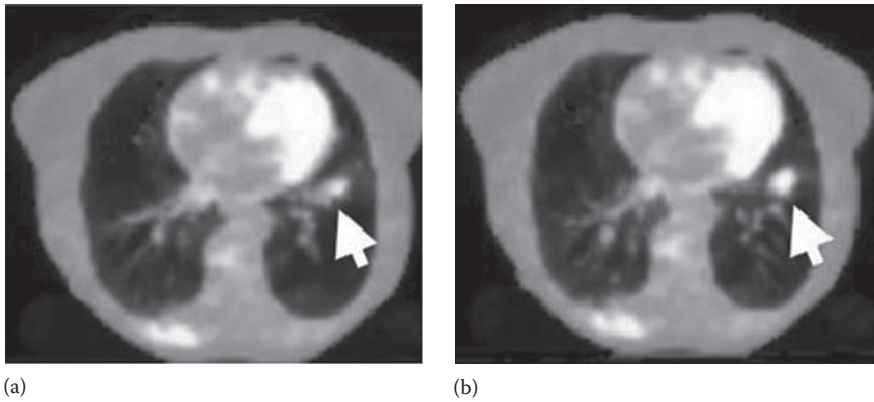


FIGURE 15.9

(See color insert.) Sampled transaxial fused PET/CT images demonstrated a thoracic lesion of a patient in (a) standard nongated PET acquisition, and (b) 4D PET/CT acquisition. (Reprinted from Nehmeh, S.A. et al., *Med. Phys.*, 2004, 31(12), 3179. With permission.)

In principle, it is better to utilize all PET information from the whole respiratory cycle instead of only one phase. One method to achieve this goal is to transform each respiratory PET bin to a referenced target bin that corresponds optimally to a matched CT phase from the gated CT data before attenuation correction (Figure 15.10). Several researchers used the motion vectors derived from gated CT and/or gated PET using different registration methods to guide the transformations, and there are two main categories of these applications.

1. Cardiac imaging

The movement of the heart due to breathing is difficult to model. It can be approximated by a six-parameter rigid transformation

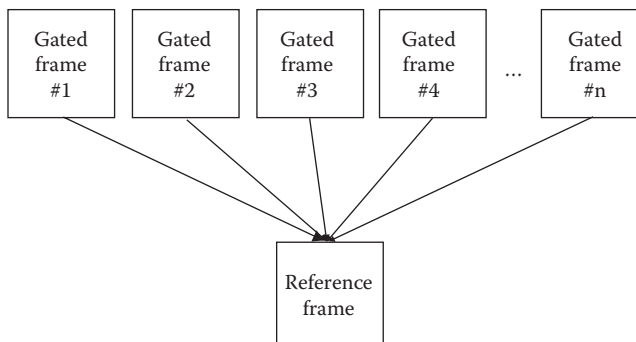


FIGURE 15.10

In 4D PET/CT gated schemes with registration, PET images are reconstructed using information from the complete dataset by registering all the frames to the reference frame.

with simple translational and rotational steps [64,65]. Livieratos et al. used this algorithm to reposition the heart to a referenced bin using the list-mode projection data before reconstruction [66]. The rigid motion was calculated from the simulated six PET respiratory gates of the digitized phantom. Substantial respiratory motion compensation in the myocardium was observed in the reconstructed images as compared with the ones without transformation in the list-mode data. Recovery of uptake contrast especially in the defect, apical, and basal myocardial areas were clearly demonstrated using the proposed method. McQuaid et al. proposed a realignment method to register a single CT with different gated PET frames, based on a rigid registration of the heart and a statistical shape model of the diaphragm [67]. Their patient studies showed that this technique led to PET reconstructed images that were closer to those with attenuation correction using a corresponding gated CT. The improved diaphragm matching between PET and CT images resulted in better quantitative accuracy. Klein et al. [68] indicated that an affine model may provide better registrations and motion correction than the technique restricted to the six-parameter rigid body assumption. Affine linear transform algorithm is a rigid motion transform for shear and compression, which is appropriate for deformation of the heart especially at the right coronary artery and left ventricle [65]. Although only small improvements were observed after performing affine model as compared to the rigid transformation model, further improvements are expected in next-generation PET scanners with better system resolution.

2. Lung imaging

Lung motion due to respiration is nonrigid in nature, and the deformation amplitude of the lungs during respiration is larger than that of the heart. Thus, CT attenuation maps are not always coregistered to PET images, especially at the lower thorax and diaphragm where large deformations often happen. This will lead to inaccurate PET reconstructed images. Therefore, for lung imaging, nonrigid motion correction algorithms would be superior to rigid motion correction algorithms.

Thorndyke et al. proposed a retrospective stacking method [69] for gated PET image processing. They retrospectively grouped all the gated PET images into several bins along measured amplitude of the respiratory cycle using RPM. These bins were then registered one-by-one to a referenced bin through B-spline deformable transformation, and then stacked and averaged to form a composite image. This method yielded reduced blurring and increased SNR in the reconstructed images as compared to conventional gated

4D PET/CT. Dawood et al. used the optical flow method (OFM) to calculate 3D motion vectors from the gated PET images [26]. For gated PET, OFM was further developed for estimating motion vectors between any bin and the target bin. The reconstructed image contained all PET information with minimal motion, leading to more accurate attenuation correction and quantification. The improvement of contrast slightly varied for lung lesion of different locations and sizes [33], and the smaller lesions (7 and 11 mm) suffered from more significant partial volume effect (PVE) as compared to the bigger lesions [70,71].

The 4D PET/CT transform algorithm is very computationally intensive. It also requires gating hardware to support the acquisition. In the meantime, this method may not be feasible for most clinics because of the high complexity of implementation. A practical alternate is quiescent period gating [72]. Studies showed that patients tend to spend more breathing time dwelling at the end-expiration quiescent period and also breathe to the same end-expiration location [23]. These results indicated that imaging at end-expiration could reduce motion blurring, while still retaining a large fraction of detected events in PET. Based on these findings, quiescent period gating techniques retrospectively extracted only the end-expiration quiescent portion of the patient breathing cycles from the PET list mode data according to external monitored motion signal to form a single PET image volume that had the optimal signal and noise tradeoff. For attenuation correction, CT image acquired during end-expiration phase had the best match with end-expiration PET data and thus was used. This technique has been implemented in commercial PET/CT scanners.

15.4.2 Reconstruction-Based Methods

While registration-based 4D PET/CT methods process either the PET raw projection data or the reconstructed images by registering and averaging individual gated frames, motion compensation can also be done by incorporating deformations information among different frames into the iterative reconstruction process. The reconstruction-based method may lead to superior image quality than the registration-based method.

Lamare et al. [73] indicated the elastic motion correction can be integrated into the system matrix in the PET reconstruction process. If P is the system matrix that describes the PET system, the data acquisition in PET can be represented by the following equation:

$$m = Pf \tag{15.1}$$

where

m is the measured datasets and

f is the radioactive distribution at the referenced respiratory location

The 3D spatial transformations for correcting the respiratory motion were obtained from the simulated 4D CT data. Deformation matrices were derived among all individual frames (acquired at time t) and the referenced frame of the full exhalation (acquired at time t_0)

$$m_t = P_t f \quad (15.2)$$

where

m_t is the measured datasets at variable time t

P_t is the system matrices at variable time t

f is the radioactive distribution at time t_0 .

This elastic-based respiratory motion correction can be integrated into the one-pass list-mode expectation-maximization (OPL-EM) algorithm

$$f^{k+1} = \frac{f^k}{S} \sum_N P_t^T \frac{1}{P_t f^k} \quad (15.3)$$

where

S is the sensitivity image used to correct for attenuation and normalization and

N is the number of temporal gated frames

The results showed that incorporating the spatial transformation into reconstruction leads to a superior contrast of 20%–30% on average in the recovered lesion, in comparison to registering the reconstructed images of individual gated frames. Thus, motion-free PET images would be obtained after the attenuation correction with the end-expiration CT data. Similar results were also demonstrated in [74,75].

Grotus et al. [76] introduced the 4D joint-estimation algorithm to form a new 4D-OS (ordered subset)-EM reconstruction for gated PET images. They assumed the activity distribution at time t $f(i, t)$ of each voxel i can be written as a linear combination of a small number (N) of temporal basis functions

$$f(i, t) = \sum_{n=1}^N b_n(t) w_n(i) \quad (15.4)$$

Only the N basis functions $b_n(t)$ and the weights of each voxel $w_n(i)$ or these basis functions needed to be estimated. As the basis functions span the whole temporal range, basis functions and weight image functions were updated iteratively as in the OS-EM technique

$$w^{k+1} = \frac{w^k}{S} \sum_N Cb_i^T P_i^T \frac{1}{Cb_i P_i w^k} \quad (15.5)$$

$$b^{k+1} = \frac{b^k}{S} \sum_N Cw_i^T P_i^T \frac{1}{Cw_i P_i b^k} \quad (15.6)$$

where

S is the sensitivity image used to correct for attenuation and normalization

P_i is the system matrices at variable time t

Cb_i and Cw_i are the matrices used to connect the basis function $b_n(t)$ and the weight function $w_n(i)$.

The N basis functions $b_n(t)$ were initialized as sinusoids with all sinusoids having the same frequency but with different phases. The weight image functions $w_n(i)$ are initialized as uniform images. The weight image functions and the basis functions were both updated for every subset by running Equations 15.5 and 15.6 successively.

The advantage of this method was that it did not need any estimation of the deformation between gated PET images and image registrations. This method did not require 4D CT data, and radiation dose was significantly reduced. The 4D reconstruction incorporating motion compensation can yield a better trade-off between SNR and bias in estimating the activity for moving tumor than nongated and independent gating without registration methods [76].

The approaches mentioned earlier usually lead to low-noise image of a gated frame, which still contains intraframe motion, and thus are not completely motion-free. Liu et al. proposed to use the correlation between internal organ motion and external monitored motion to derive the complete rigid motion information of a tumor or an internal organ, such as heart, at high temporal resolution [75]. The derived internal motion information was then incorporated into list mode reconstruction to generate event-by-event motion corrected images without intraframe motion and noise amplification [77]. The referenced respiratory location that all list mode events were registered to was chosen to match with the acquired helical CT images [78]. Since this approach is designed to correct motion for a known target organ or tumor with assumed rigid motion, it is better suited for quantification applications of a known object rather than detecting unknown abnormalities.

15.5 Deconvolution PET/CT

Deconvolution techniques have been utilized successfully to remove the blurring of medical images, such as CT [79], MRI [80], and solve the PVE problem in PET [81,82]. This technique could reduce the inherent motion blur in PET images without any gating.

Naqa et al. suggested that the motion blur of the lung lesion can be modeled as an convolution between the true PET image and the local motion blurring kernel (MBK) [83]

$$I_{obs} = I_{true} \otimes \text{MBK}.$$

where

- I_{obs} was the observed blurred PET image,
- I_{true} as the true PET image
- \otimes represented the convolution process

There were three steps for their method: (i) estimation of the breathing motion model from 4D CT data; (ii) conversion of the motion estimates into the MBK; (iii) deconvolution based on an EM iterative algorithm using the MBK. The clinical results showed this method was promising for either large or small tumors.

Chang et al. proposed a joint respiratory motion and PVE correction approach to improve the accuracy of PET image quantification [84]. In this regard, the observed PET image can be modeled as the convolution between PVE-blurred PET image and the MBK (Figure 15.11)

$$I_{obs} = (I_{true} \otimes \text{PSF} + n) \otimes \text{MBK}$$

where n is the additive noise. This method was implemented for both phantom and patient studies. The authors indicated that this technique has the potential to improve the accuracy of PET quantification in clinical environment as both PVE and respiratory motion have an effect of decreasing the tumor SUV based on their results.

There are three limitations for respiratory motion deblurring with deconvolution method: (i) Deconvolution works on the aggregated reconstructed images, but not on phase by phase basis. If the tumor moved in a nonrigid way, which sometimes happens, the over- or underestimation in tumor activity concentration can lead to inaccurate PET image quantification. (ii) This method is applied at a regional level, but not for the entire image. It can only correct the motion blur in a tumor-related region rather than the whole PET image, since most body structures move with a different pattern as compared to the tumor. (iii) Deconvolution process generally amplifies image noise, and thus may affect image quality and quantitative accuracy.

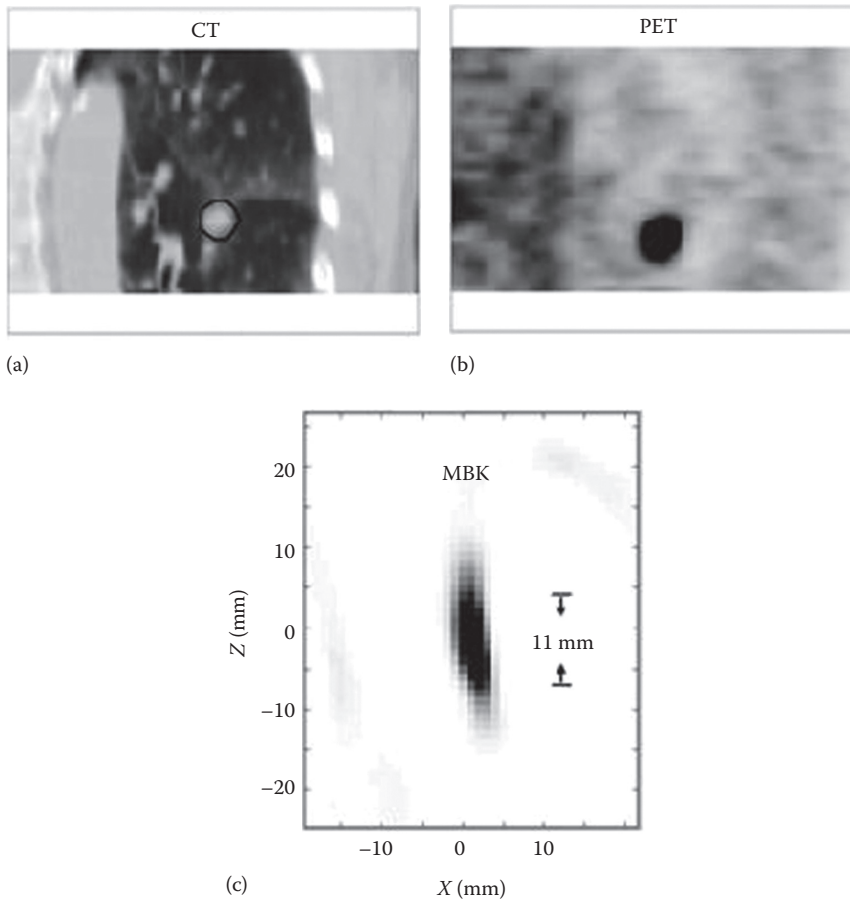


FIGURE 15.11

(a) The coronal view of the sampled 4D CT image, (b) the coronal view of the uncorrected PET image, and (c) the MBK estimated from 4D CT. (Reprinted from Chang, G. et al., *Med. Phys.*, 2010, 37(12), 6221. With permission.)

15.6 Conclusion

The CT-based method is better than the conventional ^{68}Ge -based transmission method for attenuation correction in PET in many aspects. However, it is hampered by respiratory artifacts. Several approaches to correct these artifacts in PET/CT images have been reviewed.

Attenuation correction with breath-hold CT is the easiest way to obtain the reconstructed PET image. Among different breathing patterns, normal

end-expiration breath-hold CT shows the best result. However, patient compliance is critical to ensure the breath-hold duration. Some patients with heart disease or lung tumor usually do not have normal cardiopulmonary function, and it is hard to coach them to hold and release their breath consistently over many cycles during the examination.

With the computational capability of advanced computers, pre- and postprocessing techniques are preferred to achieve a better PET/CT registration. Further averaging the CT data over one or many respiratory cycles matches the PET data better. However, PET attenuation correction with slow CT results in severe inconsistent artifacts in the reconstructed image. Low-pitch CT and CACT overcome the inconsistent artifacts with the expense of higher radiation dose, which is a significant concern for patient safety. An alternative method using IACT for attenuation correction is introduced to further reduce radiation dose with similar image quality of CACT, but none of these methods can reduce the inherent motion blur in PET images.

Gated 4D PET/CT is an ongoing research technique to eliminate spatial blurring of the emission data. However, it takes huge amount of efforts for data acquisition and processing, and it may only be feasible for research institutions at this stage. Quiescent period gating is a practical approach to reduce motion blur with minimal noise increase and has been implemented in commercial scanners. To further improve image quality of reconstructed images, reconstruction-based method and deconvolution-based method are proposed. However, these methods need further evaluation on the clinical patients.

Each respiratory artifact reduction technique has its own advantages and disadvantages, and the optimum approach may probably be task- or patient-dependent. While improving image quality is important, the actual implementation of the respiratory artifact reduction technique highly depends on the robustness and complexity of the clinical setup.

Acknowledgments

This work was supported in parts by the Multi-Year Research Grants (MYRG185(Y1-L3)-FST11-MSP & MYRG077(Y1-L2)-FST12-MSP) of University of Macau, Macau, an internal support from the Department of Diagnostic Radiology of Yale University, CTSA Grant (UL1 RR024139) from the National Institutes of Health (NIH), USA, and a research contract from Siemens Medical Solutions.

References

1. Beyer T, Townsend DW, Brun T, Kinahan PE, Charron M, Roddy R, et al. A combined PET/CT scanner for clinical oncology. *J Nucl Med*. 2000 Aug;41(8):1369–1379.
2. Townsend DW, Beyer T, Kinahan P, Meltzer CC, Brun T, Nutt R. The SMART scanner: A combined PET/CT tomograph for clinical oncology. *Radiology*. 1998 Nov;209P:169–170.
- AQ1 3. Chang LT. A method for attenuation correction in radionuclide computed tomography. *IEEE Trans Nucl Sci*. 1978;25(1):638–643.
4. Bergstrom M, Litton J, Eriksson L, Bohm C, Blomqvist G. Determination of object contour from projections for attenuation correction in cranial positron emission tomography. *J Comput Assist Tomogr*. 1982;6(2):365–372.
5. Meikle SR, Bailey DL, Hooper PK, Eberl S, Hutton BF, Jones WF. Simultaneous emission and transmission measurements for attenuation correction in whole-body PET. *J Nucl Med*. 1995 Sep;36(9):1680–1688.
6. Meikle SR, Dahlbom M, Cherry SR. Attenuation correction using count-limited transmission data in positron emission tomography. *J Nucl Med*. 1993 Jan;34(1):143–144.
7. Kinahan PE, Hasegawa BH, Beyer T. X-ray-based attenuation correction for positron emission tomography/computed tomography scanners. *Semin Nucl Med*. 2003 Jul;33(3):166–179.
8. Kinahan P, Townsend DW, Beyer T, Sashin D. Attenuation correction for a combined 3D PETCT scanner. *Med Phys*. 1998;25(10):2046–2053.
9. Nakamoto Y, Osman M, Cohade C, Marshall LT, Links JM, Kohlmyer S, et al. PET/CT: Comparison of quantitative tracer uptake between germanium and CT transmission attenuation-corrected images. *J Nucl Med*. 2002 Sep 1;43(9):1137–1143.
10. Burger C, Goerres G, Schoenes S, Buck A, Lonn AHR, von Schulthess GK. PET attenuation coefficients from CT images: Experimental evaluation of the transformation of CT into PET 511-keV attenuation coefficients. *Eur J Nucl Med Mol Imaging*. 2002 Jul;29(7):922–927.
11. McCord ME, Bacharach SL, Bonow RO, Dilsizian V, Cuocolo A, Freedman N. Misalignment between PET transmission and emission scans: Its effect on myocardial imaging. *J Nucl Med*. 1992 June 1;33(6):1209–1214.
12. Beyer T, Antoch G, Blodgett T, Freudenberg LF, Akhurst T, Mueller S. Dual-modality PET/CT imaging: The effect of respiratory motion on combined image quality in clinical oncology. *Eur J Nucl Med Mol Imaging*. 2003;30(4):588–596.
13. Osman MM, Cohade C, Nakamoto Y, Wahl RL. Respiratory motion artifacts on PET emission images obtained using CT attenuation correction on PET-CT. *Eur J Nucl Med Mol Imaging*. 2003 Apr;30(4):603–606.
14. Sureshbabu W, Mawlawi O. PET/CT imaging artifacts. *J Nucl Med Technol*. 2005 Sep 1;33(3):156–161.
15. Beyer T, Bockisch A, Kühl H, Martinez M-J. Whole-body 18F-FDG PET/CT in the presence of truncation artifacts. *J Nucl Med*. 2006 Jan;47(1):91–99.
16. Goerres GW, Hany F, Kamel E, von Schulthess GK, Buck A. Head and neck imaging with PET and PET/CT: Artefacts from dental metallic implants. *Eur J Nucl Med Mol Imaging*. 2002;29(3):367–370.

17. Kamel EM, Burger C, Buck A, von Schulthess GK, Goerres GW. Impact of metallic dental implants on CT-based attenuation correction in a combined PET/CT scanner. *Eur Radiol.* 2003 Apr;13(4):724–728.
18. Antoch G, Freudenberg LS, Egelhof T, Stattaus J, Jentzen W, Debatin JF, et al. Focal tracer uptake: A potential artifact in contrast-enhanced dual-modality PET/CT Scans. *J Nucl Med.* 2002 Oct 1;43(10):1339–1342.
19. Dizendorf E, Hany TF, Buck A, von Schulthess GK, Burger C. Cause and magnitude of the error induced by oral CT contrast agent in CT-based attenuation correction of PET emission studies. *J Nucl Med.* 2003 May;44(5):732–738.
20. Gould KL, Pan T, Loghin C, Johnson NP, Guha A, Sdringola S. Frequent diagnostic errors in cardiac PET/CT due to misregistration of CT attenuation and emission PET images: A definitive analysis of causes, consequences, and corrections. *J Nucl Med.* 2007;48(7):1112–1121.
21. Erdi YE, Nehmeh SA, Pan T, Pevsner A, Rosenzweig KE, Mageras G, et al. The CT motion quantitation of lung lesions and its impact on PET-measured SUVs. *J Nucl Med.* 2004;45(8):1287–1292.
22. Pevsner A, Nehmeh SA, Humm JL, Mageras GS, Erdi YE. Effect of motion on tracer activity determination in CT attenuation corrected PET images: A lung phantom study. *Med Phys.* 2005;32(7):2358.
23. Liu C, II LAP, Alessio AM, Kinahan PE. The impact of respiratory motion on tumor quantification and delineation in static PET/CT imaging. *Phys Med Biol.* 2009;54(24):7345–7362.
24. Cook G, Wegner E, Fogelman I. Pitfalls and artifacts in FDG PET and PET/CT oncologic imaging. *Semin Nucl Med.* 2004;34(2):122–133.
25. Nehmeh SA, Erdi YE. Respiratory motion in positron emission tomography/computed tomography: A review. *Semin Nucl Med.* 2008;38(3):167–176.
26. Dawood M, Buther F, Xiaoyi J, Schafers KP. Respiratory motion correction in 3-D PET data with advanced optical flow algorithms. *IEEE Trans Med Imaging.* 2008;27(8):1164–1175.
27. Erdi YE, Nehmeh SA, Pan T, Pevsner A, Rosenzweig KE, Mageras G, et al. The CT motion quantitation of lung lesions and its impact on PET-measured SUVs. *J Nucl Med.* 2004 Aug;45(8):1287–1292.
28. Xu QS, Yuan KH, Ye DT. Respiratory motion blur identification and reduction in ungated thoracic PET imaging. *Phys Med Biol.* 2011 Jul 21;56(14):4481–4498.
29. Allen-Auerbach M, Yeom K, Park J, Phelps M, Czernin J. Standard PET/CT of the chest during shallow breathing is inadequate for comprehensive staging of lung cancer. *J Nucl Med.* 2006;47(2):298–301.
30. Beyer T, Rosenbaum S, Veit P, Stattaus J, Muller SP, Difilippo FP, et al. Respiration artifacts in whole-body (18)F-FDG PET/CT studies with combined PET/CT tomographs employing spiral CT technology with 1 to 16 detector rows. *Eur J Nucl Med Mol Imaging.* 2005 Dec;32(12):1429–1439.
31. Goerres GW, Kamel E, Seifert B, Burger C, Buck A, Hany TF, et al. Accuracy of image coregistration of pulmonary lesions in patients with non-small cell lung cancer using an integrated PET/CT system. *J Nucl Med.* 2002;43(11):1469–1475.
32. de Juan R, Seifert B, Berthold T, von Schulthess GK, Goerres GW. Clinical evaluation of a breathing protocol for PET/CT. *Eur Radiol.* 2004;14(6):1118–1123.
33. Hamill JJ, Bosmans G, Dekker A. Respiratory-gated CT as a tool for the simulation of breathing artifacts in PET and PET/CT. *Med Phys.* 2008;35(2):576.

34. Senan S, De Ruyscher D, Giraud P, Mirimanoff R, Budach V. Literature-based recommendations for treatment planning and execution in high-dose radiotherapy for lung cancer. *Radiother Oncol.* 2004;71(2):139–146.
35. Vogel WV, van Dalen JA, Wiering B, Huisman H, Corstens FHM, Ruers TJM, et al. Evaluation of image registration in PET/CT of the liver and recommendations for optimized imaging. *J Nucl Med.* 2007;48(6):910–919.
36. Nehmeh SA, Erdi YE, Meirelles GSP, Squire O, Larson SM, Humm JL, et al. Deep-inspiration breath-hold PET/CT of the thorax. *J Nucl Med.* 2007 Jan 2007;48(1):22–26.
37. Meirelles GSP, Erdi YE, Nehmeh SA, Squire OD, Larson SM, Humm JL, et al. Deep-inspiration breath-hold PET/CT: Clinical findings with a new technique for detection and characterization of thoracic lesions. *J Nucl Med.* 2007 May;48(5):712–719.
38. Torizuka T, Tanizaki Y, Kanno T, Futatsubashi M, Yoshikawa E, Okada H, et al. Single 20-second acquisition of deep-inspiration breath-hold PET/CT: Clinical feasibility for lung cancer. *J Nucl Med.* 2009;50(10):1579–1584.
39. Yamaguchi T, Ueda O, Hara H, Sakai H, Kida T, Suzuki K, et al. Usefulness of a breath-holding acquisition method in PET/CT for pulmonary lesions. *Ann Nucl Med.* 2009;23(1):65–71.
40. Nagamachi S, Wakamatsu H, Kiyohara S, Fujita S, Futami S, Arita H, et al. The reproducibility of deep-inspiration breath-hold 18F-FDG PET/CT technique in diagnosing various cancers affected by respiratory motion. *Ann Nucl Med.* 2010;24(3):171–178.
41. Kalender WA, Seissler W, Klotz E, Vock P. Spiral volumetric CT with single-breath-hold technique, continuous transport, and continuous scanner rotation. *Radiology.* 1990 July 1, 1990;176(1):181–183.
42. Kalender WA. X-ray computed tomography. *Phys Med Biol.* 2006;51(13):R29.
43. Lagerwaard FJ, Van Sornsen de Koste JR, Nijssen-Visser MRJ, Schuchhard-Schipper RH, Oei SS, Munne A, et al. Multiple “slow” CT scans for incorporating lung tumor mobility in radiotherapy planning. *Int J Radiat Oncol Biol Phys.* 2001;51(4):932–937.
44. van Sornsen de Koste JR, Lagerwaard FJ, Schuchhard-Schipper RH, Nijssen-Visser MRJ, Voet PWJ, Oei SS, et al. Dosimetric consequences of tumor mobility in radiotherapy of stage I non-small cell lung cancer—an analysis of data generated using ‘slow’ CT scans. *Radiother Oncol.* 2001;61(1):93–99.
45. Nye JA, Esteves F, Votaw JR. Minimizing artifacts resulting from respiratory and cardiac motion by optimization of the transmission scan in cardiac PET/CT. *Med Phys.* 2007;34(6):1901.
46. Pan T, Mawlawi O, Nehmeh SA, Erdi YE, Luo D, Liu HH, et al. Attenuation Correction of PET images with respiration-averaged CT images in PET/CT. *J Nucl Med.* 2005 Sep 1;46(9):1481–1487.
47. Pan T, Lee T-Y, Rietzel E, Chen GTY. 4D-CT imaging of a volume influenced by respiratory motion on multi-slice CT. *Med Phys.* 2004;31(2):333.
48. Pan T, Mawlawi O, Luo D, Liu HH, Chi P-cM, Mar MV, et al. Attenuation correction of PET cardiac data with low-dose average CT in PET/CT. *Med Phys.* 2006;33(10):3931.
49. Cook RA, Carnes G, Lee TY, Wells RG. Respiration-averaged CT for attenuation correction in canine cardiac PET/CT. *J Nucl Med.* 2007 May;48(5):811–818.
50. Alessio AM, Kohlmyer S, Branch K, Chen G, Caldwell J, Kinahan P. Cine CT for attenuation correction in cardiac PET/CT. *J Nucl Med.* 2007;48(5):794–801.


51. Tzung-Chi H, Mok GSP, Wang S-J, Wu T-H, Zhang G. Attenuation correction of PET images with interpolated average CT for thoracic tumors. *Phys Med Biol.* 2011;56(8):2559.
52. Guerrero T, Zhang G, Huang T-C, Lin K-P. Intrathoracic tumour motion estimation from CT imaging using the 3D optical flow method. *Phys Med Biol.* 2004;49(17):4147–4161.
53. Lujan AE, Balter JM, Haken RKT. A method for incorporating organ motion due to breathing into 3D dose calculations in the liver: Sensitivity to variations in motion. *Med Phys.* 2003;30(10):2643–2649.
54. Mok GSP, Sun T, Wu T-H, Chang M-B, Huang T-C. Interpolated average CT for attenuation correction in PET—A simulation study. IEEE Nuclear Science Symposium and Medical Imaging Conference Record, Valencia, Spain, 2011; pp. 4121–4125.
55. Sun T, Wu T-H, Wu N-Y, Mok GSP. Low dose interpolated average CT for PET/CT attenuation correction using an Active Breathing Controller (ABC) paper accepted for presentation in IEEE Nuclear Science Symposium Medical Imaging Conference, Anaheim, CA, Oct 28–Nov 3, 2012.
56. Picard Y, Thompson CJ. Motion correction of PET images using multiple acquisition frames. *IEEE Trans Med Imaging.* 1997;16(2):137–144.
57. Nehmeh SA, Erdi YE, Ling CC, Rosenzweig KE, Squire OD, Braban LE, et al. Effect of respiratory gating on reducing lung motion artifacts in PET imaging of lung cancer. *Med Phys.* 2002;29(3):366.
58. Boucher L, Rodrigue S, Lecomte R, Bénard F. Respiratory gating for 3-dimensional PET of the thorax: Feasibility and initial results. *J Nucl Med.* 2004 February 1;45(2):214–219.
59. Nehmeh SA, Erdi YE, Pan T, Pevsner A, Rosenzweig KE, Yorke E, et al. Four-dimensional (4D) PET/CT imaging of the thorax. *Med Phys.* 2004;31(12):3179.
60. Ponisch F, Richter C, Just U, Enghardt W. Attenuation correction of four dimensional (4D) PET using phase-correlated 4D-computed tomography. *Phys Med Biol.* 2008 Jul 7;53(13):N259–N268.
61. Wells RG, Ruddy TD, DeKemp RA, DaSilva JN, Beanlands RS. Single-phase CT aligned to gated PET for respiratory motion correction in cardiac PET/CT. *J Nucl Med.* 2010;51(8):1182–1190.
62. Nagel CCA, Bosmans G, Dekker ALAJ, Öllers MC, De Ruyscher DKM, Lambin P, et al. Phased attenuation correction in respiration correlated computed tomography/positron emitted tomography. *Med Phys.* 2006;33(6):1840.
63. Liu C, Alessio AM, Kinahan PE. Respiratory motion correction for quantitative PET/CT using all detected events with internal—external motion correlation. *Med Phys.* 2011;38(5):2715–2723.
64. McLeish K, Hill DLG, Atkinson D, Blackall JM, Razavi R. A study of the motion and deformation of the heart due to respiration. *IEEE Trans Med Imaging.* 2002;21(9):1142–1150.
65. Shechter G, Ozturk C, Resar JR, McVeigh ER. Respiratory motion of the heart from free breathing coronary angiograms. *IEEE Trans Med Imaging.* 2004;23(8):1046–1056.
66. Livieratos L, Stegger L, Bloomfield PM, Schafers K, Bailey DL, Camici PG. Rigid-body transformation of list-mode projection data for respiratory motion correction in cardiac PET. *Phys Med Biol.* 2005;50(14):3313.
67. McQuaid SJ, Lambrou T, Hutton BF. A novel method for incorporating respiratory-matched attenuation correction in the motion correction of cardiac PET-CT studies. *Physics in Medicine and Biology.* 2011 May 21;56(10):2903–2915.

AQ2

68. Klein GJ, Reutter RW, Huesman RH. Four-dimensional affine registration models for respiratory-gated PET. *IEEE Trans Nuc Sci.* 2001;48(3):756–760.
69. Thorndyke B, Schreibmann E, Koong A, Xing L. Reducing respiratory motion artifacts in positron emission tomography through retrospective stacking. *Med Phys.* [10.1118/1.2207367]. 2006;33(7):2632.
70. Soret M, Bacharach SL, Buvat I. Partial-volume effect in PET tumor imaging. *J Nucl Med.* 2007 June;48(6):932–945.
71. Visvikis D, Lamare F, Bruyant P, Boussion N, Cheze Le Rest C. Respiratory motion in positron emission tomography for oncology applications: Problems and solutions. *Nucl Instrum Methods Phys Res A.* 2006;569(2):453–457.
72. Liu C, Alessio A, Pierce L, Thielemans K, Wollenweber S, Ganin A, et al. Quiescent period respiratory gating for PET/CT. *Med Phys.* 2010;37(9):5037–5043.
73. Lamare F, Carbayo MJL, Cresson T, Kontaxakis G, Santos A, Rest CCL, et al. List-mode-based reconstruction for respiratory motion correction in PET using non-rigid body transformations. *Phys Med Biol.* 2007;52(17):5187–5204.
74. Li T, Thorndyke B, Schreibmann E, Yang Y, Xing L. Model-based image reconstruction for four-dimensional PET. *Med Phys.* 2006;33(5):1288–1298.
- AQ3 75. Qiao F, Pan T, Clark JW Jr, Mawlawi OR. A motion-incorporated reconstruction method for gated PET studies. *Phys Med Biol.* 2006;51(15):3769
76. Grotus N, Reader AJ, Stute S, Rosenwald JC, Giraud P, Buvat I. Fully 4D list-mode reconstruction applied to respiratory-gated PET scans. *Phys Med Biol.* 2009;54(6):1705.
77. Chan C, Jin X, Fung EK, Mulnix T, Carson RE, CL. Event-by-event respiratory motion correction with 3-dimensional internal-external motion correlation. paper accepted for presentation in IEEE Nuclear Science Symposium and Medical Imaging Conference, Anaheim, CA, Oct 28–Nov 3, 2012.
78. Alessio AM, Kinahan PE, Champlsey KM, Caldwell JH. Attenuation-emission alignment in cardiac PET/CT based on consistency conditions. *Med Phys.* 2010;37(3):1191–1200.
79. Ming J, Ge W, Skinner MW, Rubinstein JT, Vannier MW. Blind deblurring of spiral CT images. *IEEE Trans Med Imaging.* 2003;22(7):837–845.
80. Sourbron S, Luytjaert R, Van Schuerbeek P, Dujardin M, Stadnik T, Osteaux M. Deconvolution of dynamic contrast-enhanced MRI data by linear inversion: Choice of the regularization parameter. *Magn Reson Med.* 2004;52(1):209–213.
81. Kirov AS, Piao JZ, Schmittlein CR. Partial volume effect correction in PET using regularized iterative deconvolution with variance control based on local topology. *Phys Med Biol.* 2008;53(10):2577.
82. Faber TL, Raghunath N, Tudorascu D, Votaw JR. Motion correction of PET brain images through deconvolution: I. Theoretical development and analysis in software simulations. *Phys Med Biol.* 2009;54(3):797.
83. Naqa IE, Low DA, Bradley JD, Vicic M, Deasy JO. Deblurring of breathing motion artifacts in thoracic PET images by deconvolution methods. *Med Phys.* 2006;33(10):3587–3600.
84. Chang G, Chang T, Pan T, John W, Clark J, Mawlawi OR. Joint correction of respiratory motion artifact and partial volume effect in lung/thoracic PET/CT imaging. *Med Phys.* 2010;37(12):6221–6232.

Author Queries

[AQ1] Please confirm inserted page range detail for Ref. [3]. 

[AQ2] Please confirm inserted location detail for Ref. [54]. 

[AQ3] Please confirm inserted author name detail for Ref.  